Dynamics of Photoinduced Proton-Coupled Electron Transfer at Molecule−Semiconductor Interfaces: A Reduced Density Matrix Approach

Charulatha Venkataraman, Alexander V. Soudackov, and Sharon Hammes-Schiffer*

Department of Chemistry, 104 Chemistry Building, Pennsylvania State University, University Park, Pennsylvania 16802

Received: September 11, 2009

A theoretical model for describing the dynamics of photoinduced proton-coupled electron transfer (PCET) at molecule−semiconductor interfaces is presented. In this model, the electron is photoexcited to a molecular electronic state near the semiconductor surface, and the subsequent electron transfer to the conduction band of the semiconductor is coupled to a proton transfer reaction. The electron could be photoexcited from the ground to an excited electronic state within a dye molecule at the interface or from the defect band in the semiconductor to a molecular adsorbate layer. A model Hamiltonian is developed to describe this PCET process, and the equations of motion for the reduced density matrix elements in the basis of electron−proton vibronic states are derived. This formulation is used to calculate the time-dependent electronic and vibronic state populations for a series of model systems. These calculations provide insight into the hydrogen/deuterium isotope effect on the dynamics of the donor state population decay for ultrafast interfacial PCET. This isotope effect depends on the initial proton wavepacket and the relative time scales of the donor electronic state population decay and proton vibrational relaxation. The effects of the electronic coupling, temperature, and energy of the donor state on the population dynamics are also investigated for photoinduced interfacial electron transfer and PCET. The resulting theoretical predictions about the qualitative impact of altering system properties on the population decay time scales could be useful for designing catalysts that activate bonds containing hydrogen atoms.

I. Introduction

Photoinduced electron transfer at molecule−semiconductor interfaces is the key step in many photocatalytic and solar energy conversion processes.[1,2] Substantial experimental and theoretical efforts have been directed toward understanding photoinduced electron transfer (ET) at dye−semiconductor interfaces,[3−10] where an electron promoted to an excited electronic state of the dye molecule is injected into a semiconductor such as titanium dioxide (TiO_2). Other studies have focused on photoinduced ET in semiconductors with chemisorbed molecular overlayers containing water or methanol. In these systems, an electron is photoexcited from the defect band in the semiconductor to the molecular overlayer and is subsequently transferred back to the semiconductor conduction band through various relaxation processes.[11−18] The injection of electrons into the molecular overlayer has been observed to induce significant nuclear rearrangements and, in some cases, chemical reactions. A well-known example is photocatalytic water splitting on a TiO_2 surface.[19] Understanding the coupling between electronic and nuclear motions in these types of processes is directly relevant to the design of catalysts that activate bonds containing hydrogen atoms, which is important for the development of clean, sustainable, and renewable energy sources.

Recently, Petek and co-workers studied ultrafast interfacial proton-coupled electron transfer (PCET) in CH_3OH/TiO_2 systems comprised of methanol adsorbed on a TiO_2 surface.[16,18] In their time-resolved two-photon photoemission experiments, an electron is photoexcited from the defect band in the semiconductor to the methanol adsorbate layer, and the energy and population dynamics of the resulting "solvated" electron state in the methanol adsorbate layer are monitored. The data indicate a fast component and a slow component of the energy and population decay processes. The fast and slow components are attributed to lattice and solvent relaxation, respectively. A significant deuterium isotope effect with CH_3OD for the slow component suggests that this charge transfer process involves coupled electronic and nuclear motions. As the electron is transferred back to the semiconductor, proton transfer is hypothesized to occur between a methanol molecule and a bridging oxygen on the TiO_2 surface. Although much effort has been directed toward the development of theoretical methods to study ultrafast interfacial ET,[4−9,20−23] a rigorous theoretical framework for ultrafast interfacial PCET is still lacking.

Theoretical approaches based on the nonadiabatic golden rule formalism have been developed and applied to a wide range of homogeneous PCET reactions in solution and proteins.[24−29] These treatments have also been extended to electrochemical PCET.[30−32] A number of theoretical approaches based on the Anderson−Newns model Hamiltonian have been employed to study electrochemical ET,[33−38] electrochemical PCET,[31,39] and proton tunneling at the electrochemical interface.[40] A significant difference that arises for ultrafast photoexcited PCET is that the processes are not at equilibrium. The development of a theory to describe the nonequilibrium dynamics of ultrafast interfacial PCET processes is challenging because of the strong coupling of the charge transfer reaction to the bath representing the lattice and solvent modes, the quasicontinuum of electronic states in the semiconductor, and the quantum mechanical behavior of the transferring proton. Many of these challenges have been addressed in the context of heterogeneous ET

* Corresponding author. E-mail: shs@chem.psu.edu.

10.1021/jp908798n
Published on Web 11/19/2009

processes. Ultrafast ET in dye-sensitized TiO_2 semiconductor systems has been studied using nonadiabatic molecular dynamics[4] and various quantum dynamical methods.[5−9] In addition, electronic−vibrational dynamical processes in heterogeneous environments have been studied using time-dependent wavepacket methods[9,41−45] and the exact Green's function approach[46] with Anderson−Newns model Hamiltonians.[33,47,48] Vibrational and solvent relaxation processes in heterogeneous ET have been studied with Redfield theory[49] in the weak system−bath coupling limit.[50−54]

The objective of this work is to develop a theoretical framework for describing ultrafast interfacial PCET at molecule−semiconductor interfaces and to investigate the dynamics of these processes. This theory is designed to model two types of systems. In the first type of system, an electron is photoexcited within a dye molecule at a dye−semiconductor interface, and in the second type of system, an electron is photoexcited from the defect band in the semiconductor to a molecular adsorbate layer. In both cases, the transfer of the photoexcited electron to the conduction band of the semiconductor is coupled to proton motion. Our formulation is based on a variation of the Anderson−Newns−Schmickler model Hamiltonian[33,47,48] to describe the electron−proton system in the presence of a harmonic bath representing the lattice and solvent modes. We derive the equations of motion for the time-dependent reduced density matrix (RDM) elements of the system using the Redfield formalism, incorporating strong coupling between the transferring electron and the bath through a canonical transformation of the Hamiltonian.[55−57] The propagation of the RDM equations of motion enables the analysis of the population dynamics of the electronic states, as well as the associated proton vibrational states. Recently, we have used this formalism to study photoinduced homogeneous PCET.[58]

An outline of this article is as follows: In section IIA, we present a model Hamiltonian that describes photoinduced heterogeneous PCET reactions and perform a canonical transformation that enables the treatment of strong coupling between the electronic states and the bath. In section IIB, we apply the reduced density matrix (RDM) formalism to the canonically transformed model Hamiltonian and obtain the master equations for the populations of the electron−proton vibronic states. Section IIC provides details about the calculation of the bath correlation function and the discretization of the conduction band states. In section IIIA, we present the results of our calculations for PCET processes, focusing on the H/D isotope effect and the effects of the donor electronic state energy, temperature, and electronic coupling on the population dynamics. Section IIIB presents the corresponding results for the ET process. Concluding remarks are presented in section IV.

II. Theory

IIA. Model Hamiltonian for Ultrafast Interfacial Proton-Coupled Electron Transfer. In this subsection, we present a model Hamiltonian describing ultrafast PCET at molecule−semiconductor interfaces using an extension of the Anderson−Newns model Hamiltonian.[33,47,48] In this model, the electron is photoexcited to a molecular electronic state near the semiconductor surface, and the subsequent electron transfer to the conduction band of the semiconductor is coupled to a proton transfer reaction. The electron could be photoexcited from the ground state to an excited electronic state within a dye molecule at the interface or from the defect band in the semiconductor to a solvated electron state in the molecular adsorbate layer. We model this process using a single donor electronic state and a quasicontinuum of acceptor states in the conduction band. The donor electronic state, also denoted the molecular electronic state, corresponds to either an excited electronic state in the dye molecule or a solvated electron state in the molecular adsorbate layer. For simplicity, we assume that the initial electronic state prior to photoexcitation is uncoupled from both the donor and acceptor electronic states.

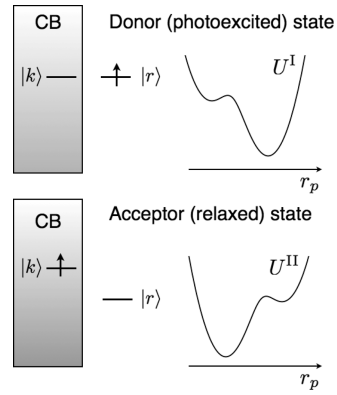

Figure 1. Schematic illustration of the donor electronic state $|r\rangle$ and an acceptor electronic state $|k\rangle$ in the conduction band of the semiconductor. The associated proton potentials $U^{\mathrm{I}}(r_{\mathrm{p}})$ and $U^{\mathrm{II}}(r_{\mathrm{p}})$ are also depicted.

Figure 1 depicts the essential characteristics of this model system. The molecular one-electron state is denoted $|r\rangle$ with energy ϵ_r, and the quasicontinuum of one-electron states for the electrode is denoted by $\{|k\rangle\}$ with energies ϵ_k. The operators $\hat{c}_r^\dagger$, $\hat{c}_r$, $\hat{c}_k^\dagger$, and $\hat{c}_k$ are the fermionic creation and annihilation operators for these electronic states. The coupling between the molecular electronic state and the semiconductor electronic states is denoted V_{rk} and is assumed to be independent of the nuclear degrees of freedom. The proton potential is $U^{\mathrm{I}}(r_{\mathrm{p}})$ when the molecular electronic state $|r\rangle$ is occupied and $U^{\mathrm{II}}(r_{\mathrm{p}})$ when the molecular electronic state $|r\rangle$ is unoccupied, where r_{p} is the proton coordinate. The proton potential is assumed to depend on only the occupation of the molecular electronic state and to be independent of the solvent coordinates, in contrast to the electrochemical PCET Hamiltonian proposed in ref 39. We also neglect the proton donor−acceptor vibrational motion, which was included in the vibronic model Hamiltonian proposed in ref 31. The environmental degrees of freedom, which could include the lattice phonon modes, the intramolecular vibrations of the redox-active molecule, and the surrounding solvent molecules, are modeled as a harmonic bath, where x_i and p_i are the position and momentum coordinates, respectively, of the ith harmonic oscillator mode with masses m_i and frequencies ω_i. The bath degrees of freedom are assumed to be coupled to the molecular electronic state with coupling constants c_i.

The Hamiltonian of the entire system has the form

$$\hat{H} = \hat{T}_{\mathrm{p}} + [\epsilon_r + U^{\mathrm{I}}(r_{\mathrm{p}})]\hat{c}_r^\dagger\hat{c}_r + \sum_k [\epsilon_k + U^{\mathrm{II}}(r_{\mathrm{p}})]\hat{c}_k^\dagger\hat{c}_k + \sum_k (V_{rk}\hat{c}_r^\dagger\hat{c}_k + V_{rk}^*\hat{c}_k^\dagger\hat{c}_r) + \sum_i \left[\frac{p_i^2}{2m_i} + \frac{m_i\omega_i^2}{2}\left(x_i + \hat{n}_r\frac{c_i}{m_i\omega_i^2}\right)^2\right] \quad (1)$$

where the number operator associated with the donor state is $\hat{n}_r = \hat{c}_r^\dagger\hat{c}_r$ and $\hat{T}_{\mathrm{p}}$ is the kinetic energy of the proton. The system−bath coupling is described by the spectral density function:[59]

$$J(\omega) = \frac{\pi}{2}\sum_i \frac{c_i^2}{m_i\omega_i}\delta(\omega - \omega_i) \quad (2)$$

This Hamiltonian can be rewritten in terms of the harmonic oscillator ladder operators $\hat{b}_i^\dagger$ and $\hat{b}_i$:

$$\hat{H} = \hat{T}_p + [\epsilon_r + U^I(r_p)]\hat{c}_r^\dagger\hat{c}_r + \sum_k [\epsilon_k + U^{II}(r_p)]\hat{c}_k^\dagger\hat{c}_k + \sum_k (V_{rk}\hat{c}_r^\dagger\hat{c}_k + V_{rk}^*\hat{c}_k^\dagger\hat{c}_r) + \sum_i \hbar\omega_i\left(\hat{b}_i^\dagger\hat{b}_i + \frac{1}{2}\right) + \hat{n}_r\sum_i \frac{\hbar c_i}{\sqrt{2\hbar m_i\omega_i}}(\hat{b}_i^\dagger + \hat{b}_i) + \hat{n}_r^2\sum_i \frac{c_i^2}{2m_i\omega_i^2} \quad (3)$$

To capture the effect of the strong interaction between the electron and the bath modes, we apply the small polaron transformation[60] to the Hamiltonian in eq 3 to obtain

$$\tilde{H} = e^{-\hat{v}\hat{c}_r^\dagger\hat{c}_r\hat{v}}\hat{H}e^{\hat{v}\hat{c}_r^\dagger\hat{c}_r\hat{v}} \quad (4)$$

where

$$\hat{v} = -\sum_i \frac{c_i}{\sqrt{2\hbar m_i\omega_i^3}}(\hat{b}_i^\dagger - \hat{b}_i) \quad (5)$$

The transformed Hamiltonian can be partitioned as

$$\tilde{H} = \hat{H}_S + \hat{H}_B + \hat{V} \quad (6)$$

where the system Hamiltonian is

$$\hat{H}_S = \hat{T}_p + [\epsilon_r + U^I(r_p)]\hat{c}_r^\dagger\hat{c}_r + \sum_k [\epsilon_k + U^{II}(r_p)]\hat{c}_k^\dagger\hat{c}_k \quad (7)$$

the bath Hamiltonian is

$$\hat{H}_B = \sum_i \hbar\omega_i\left(\hat{b}_i^\dagger\hat{b}_i + \frac{1}{2}\right) \quad (8)$$

and the interaction term is the bath-dressed electronic coupling[61]

$$\hat{V} = \sum_k V_{rk}e^{-\hat{v}}\hat{c}_r^\dagger\hat{c}_k + V_{rk}^*e^{\hat{v}}\hat{c}_k^\dagger\hat{c}_r \quad (9)$$

Because this model does not include direct coupling between the proton vibrational mode and the bath, it does not include a direct mechanism for proton vibrational relaxation. On the other hand, the proton vibrational mode is indirectly coupled to the bath because the proton vibrational mode is coupled to the electronic states, which, in turn, are coupled to the bath. Thus, this model includes an indirect mechanism for proton vibrational relaxation through nonadiabatic transitions between the donor and acceptor states. Typically, the bath is more strongly coupled to the electron transfer reaction than to the proton transfer reaction, so the proton vibrational relaxation is expected to occur on a faster time scale for the indirect mechanism than for the direct mechanism. As a result, the neglect of the direct coupling between the proton vibrational mode and the bath does not significantly impact the ultrafast dynamical relaxation of the donor electronic state population.

IIB. Reduced Density Matrix Formalism for Ultrafast Interfacial PCET. In this subsection, we describe the application of the reduced density matrix (RDM) formalism to the model Hamiltonian defined in the previous subsection. The state of the overall system and bath at any time t is described by the total density matrix $\hat{\rho}(t)$, and the time evolution of this density matrix is given by the quantum Liouville equation

$$\frac{\partial}{\partial t}\hat{\rho}(t) = -\frac{i}{\hbar}[\hat{H},\hat{\rho}(t)] \quad (10)$$

The reduced density matrix, which describes the state of only the system, is constructed by taking a trace over the bath variables: $\hat{\sigma}(t) = \mathrm{tr}_B[\hat{\rho}(t)]$. When the bath relaxation is rapid in comparison to the system dynamics, the bath can be assumed to be in thermal equilibrium throughout the process, and the bath density matrix is given as $\hat{\rho}_B = e^{-\beta\hat{H}_B}/\mathrm{tr}(e^{-\beta\hat{H}_B})$. The interaction term is treated perturbatively up to second order, and the equations of motion of the RDM are obtained in the basis of system eigenstates defined as $\hat{H}_S|\mu\rangle = E_\mu|\mu\rangle$. The matrix elements of the RDM in this basis are $\sigma_{\mu\nu}(t) = \langle\mu|\hat{\sigma}(t)|\nu\rangle$, and their equations of motion are known as the Redfield equations in the literature.[55,57] These equations of motion can be further simplified by employing the secular approximation,[55,56] which decouples the equations of motion for the diagonal (i.e., population) and off-diagonal (i.e., coherence) elements of the RDM. The resulting equations of motion for the diagonal RDM elements are known as the Pauli master equations.[56]

We apply this RDM formalism to the canonically transformed Hamiltonian $\tilde{H}$ given in eq 6. In this case, the bath-dressed electronic coupling term is treated perturbatively. Note that, typically, the RDM formalism (i.e., Redfield theory) is restricted to the treatment of weak system−bath coupling because the perturbative term is assumed to be the system−bath coupling. Because of the canonical transformation described in subsection IIA, however, we are able to treat the strong system−bath coupling case with this formalism. Our perturbative treatment is valid for all finite temperatures and for large magnitudes of the system−bath coupling strength if the bare electronic coupling element V_{rk} is reasonably small.

In this formulation, the RDM of the system is calculated in the electron−proton vibronic basis. The proton vibrational states when the electron is in the donor state (I) or any of the acceptor states (II) are obtained by solving the following Schrödinger equations:

$$\begin{aligned}[\hat{T}_p + U^I(r_p)]\chi_\mu^I(r_p) &= E_\mu^I\chi_\mu^I(r_p)\\ [\hat{T}_p + U^{II}(r_p)]\chi_\nu^{II}(r_p) &= E_\nu^{II}\chi_\nu^{II}(r_p)\end{aligned} \quad (11)$$

The eigenstates of the system Hamiltonian are denoted $|r\rangle|\chi_\mu^I\rangle$ and $|k\rangle|\chi_\nu^{II}\rangle$ when the electron is in the molecular donor state and in the kth conduction band acceptor state, respectively. The diagonal matrix elements of the RDM in the electron−proton vibronic basis are denoted $\sigma_{r\mu,r\mu}(t)$ and $\sigma_{k\nu,k\nu}(t)$, which correspond to the populations of vibronic states $|r\rangle|\chi_\mu^I\rangle$ and $|k\rangle|\chi_\nu^{II}\rangle$, respectively.

Using the formalism described in ref 58, the equations of motion of the diagonal RDM elements are given by

$$\begin{aligned}\dot{\sigma}_{r\mu,r\mu}(t) &= \sum_{k,\nu} W_{r\mu,k\nu}(t)\,\sigma_{k\nu,k\nu}(t) - \sum_{k,\nu} W_{k\nu,r\mu}(t)\,\sigma_{r\mu,r\mu}(t)\\ \dot{\sigma}_{k\nu,k\nu}(t) &= \sum_{\mu} W_{k\nu,r\mu}(t)\,\sigma_{r\mu,r\mu}(t) - \sum_{\mu} W_{r\mu,k\nu}(t)\,\sigma_{k\nu,k\nu}(t)\end{aligned} \quad (12)$$

where $W_{r\mu,k\nu}(t)$ is the time-dependent probability of transition from vibronic state $|k\rangle|\chi_\nu^{II}\rangle$ to vibronic state $|r\rangle|\chi_\mu^I\rangle$ and $W_{k\nu,r\mu}(t)$ specifies the reverse transition probability.[56] Employing the stationary Redfield tensor approximation,[62] the transition probabilities are expressed as

$$W_{r\mu,kv} = \frac{1}{\hbar^2}|V_{rk}|^2|\langle\chi_v^{II}|\chi_\mu^{I}\rangle|^2 \int_{-\infty}^{\infty} d\tau\, e^{-i(\epsilon_r-\epsilon_k+E_\mu^I-E_v^{II})\tau/\hbar}\langle e^{\hat{v}(\tau)}e^{-\hat{v}(0)}\rangle$$
$$W_{kv,r\mu} = \frac{1}{\hbar^2}|V_{rk}|^2|\langle\chi_v^{II}|\chi_\mu^{I}\rangle|^2 \int_{-\infty}^{\infty} d\tau\, e^{i(\epsilon_r-\epsilon_k+E_\mu^I-E_v^{II})\tau/\hbar}\langle e^{\hat{v}(\tau)}e^{-\hat{v}(0)}\rangle \quad (13)$$

The populations of the molecular donor state $|r\rangle$ and the acceptor conduction band state $|k\rangle$ at time t are obtained by summing over the proton vibrational states

$$P_r(t) = \sum_\mu \sigma_{r\mu,r\mu}(t), \quad P_k(t) = \sum_\nu \sigma_{kv,kv}(t) \quad (14)$$

The RDM equations of motion given in eq 12 can be solved if the initial populations of all vibronic states are specified. At zero time, the laser pulse instantaneously excites an electron to the molecular donor state $|r\rangle$. Note that the electron could be photoexcited from the defect band in the semiconductor or from the ground molecular electronic state. The proton potential corresponding to the electronic state prior to photoexcitation is denoted $U^0(r_p)$. Because the excitation is instantaneous, the bath is in the equilibrium configuration corresponding to the ground electronic state. Thus, although the initial proton wavepacket is created in the donor state with proton potential $U^I(r_p)$, it is still in the equilibrium configuration corresponding to the proton potential $U^0(r_p)$. This photoexcitation and the subsequent relaxation processes are illustrated in Figure 2.

The initial condition following photoexcitation corresponds to the electron in the donor electronic state $|r\rangle$ and the proton in a Boltzmann distribution of vibrational states associated with $U^0(r_p)$. The vibrational states for the potential $U^0(r_p)$ are denoted $|\chi_v^0\rangle$ with energies E_v^0. In this case, the initial reduced density matrix is

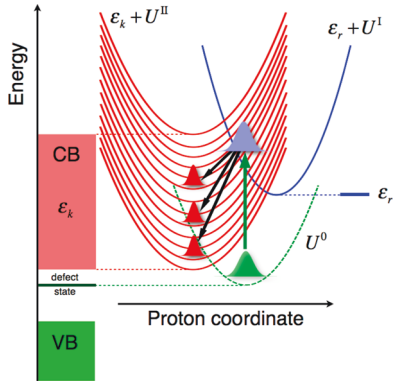

Figure 2. Schematic depiction of the photoinduced interfacial PCET model system. The proton potentials U^0, U^I, and U^{II} are depicted in green, blue, and red, respectively. The energy ϵ_r of the donor electronic state is indicated. The valence band (VB), defect states, and conduction band (CB), as well as the energy ϵ_k of the kth acceptor electronic state, are also indicated. Prior to photoexcitation, the proton wavepacket is in the electronic state with proton potential U^0. Photoexcitation from this electronic state to the donor electronic state with proton potential U^I is depicted by the green arrow. The initial wavepacket following photoexcitation is a coherent vibrational mixture in the donor electronic state. The arrows indicate the relaxation processes arising from nonadiabatic transitions between the donor and acceptor vibronic states concurrent with energy dissipation to the bath. The red wavepackets depict the final equilibrium populations in the acceptor electronic states in the conduction band of the semiconductor.

$$\hat{\sigma}(0) = |r\rangle\langle r|\frac{e^{-\beta[\hat{T}_p+U^0(r_p)]}}{Z^0} \quad (15)$$

where Z^0 is the proton vibrational partition function. The initial vibronic populations associated with the donor electronic state are

$$\sigma_{r\mu,r\mu}(0) = \sum_{v=0}^{\infty}\frac{e^{-\beta E_v^0}}{Z^0}|\langle\chi_\mu^I|\chi_v^0\rangle|^2 \quad (16)$$

and the initial vibronic populations associated with the acceptor electronic state are zero [i.e., $\sigma_{kv,kv}(0) = 0$]. If thermal effects are negligible, initially the proton is in the ground vibrational state $|\chi_0^0\rangle$ of $U^0(r_p)$, and the vibronic populations are given by the squares of the Franck−Condon overlaps of the proton vibrational wave functions [i.e., $\sigma_{r\mu,r\mu}(0) = |\langle\chi_\mu^I|\chi_0^0\rangle|^2$]. Because the photoexcited electron is in the donor electronic state at zero time, the total population of all vibronic states corresponding to the donor is unity [i.e., $P_r(0) = 1$]. Note that the initial population following photoexcitation has a nonequilibrium distribution and evolves in time toward the equilibrium distribution.

This formalism can also be used to study the process of ultrafast heterogeneous electron transfer from the donor electronic state to the conduction band of the semiconductor.[34,35] In this case, the model Hamiltonian in eq 3 reduces to the Anderson−Newns−Schmickler Hamiltonian, and the canonically transformed Hamiltonian is of the same form as given in eq 6, omitting the terms involving the proton [i.e., the terms involving $\hat{T}_p$, $U^I(r_p)$, and $U^{II}(r_p)$] in eq 7. For electron transfer, the diagonal RDM elements in the basis of system eigenstates are denoted $\sigma_{rr}(t)$ and $\sigma_{kk}(t)$, which correspond to the populations of the donor electronic state $|r\rangle$ and the acceptor conduction band states $|k\rangle$, respectively. The equations of motion for the diagonal RDM elements are given by eq 12 with the transition probabilities given by eq 13, replacing the vibronic states by electronic states (i.e., omitting the sums over vibrational states, the overlap prefactors, and the vibrational state energies in the exponential). The population dynamics for each electronic state can be obtained by the time evolution of the RDM equations of motion.

IIC. Description of the Bath and Electrode States. The bath correlation function in the transition probabilities given by eqs 13 can be evaluated exactly using the bosonic creation and annihilation operator algebra.[60] In the continuum limit of the bath modes, the bath correlation function can be expressed in terms of the spectral density as

$$\langle e^{\hat{v}(\tau)}e^{-\hat{v}(0)}\rangle = \exp[-Q(\tau)/\pi\hbar] \quad (17)$$

where

$$Q(\tau) = \int_0^\infty d\omega\,\frac{J(\omega)}{\omega^2}\left\{\coth\left(\frac{\hbar\beta\omega}{2}\right)[1-\cos(\omega\tau)] + i\sin(\omega\tau)\right\} \quad (18)$$

Note that $Q(\tau)$ is related to the energy gap correlation function[63,64] as $\langle\delta U(\tau)\ \delta U(0)\rangle = (1/\pi)(\partial^2 Q/\partial\tau^2)$, where the energy gap $U = \sum_i c_i x_i$ is the collective reaction coordinate of the harmonic bath and $\delta U(\tau) = U(\tau) - \langle U\rangle$ is the instantaneous fluctuation of the energy gap from the equilibrium average.

We define $I(\omega)$ as the Fourier transform of the bath correlation function

$$I(\omega) = \int_{-\infty}^{\infty} d\tau\, e^{i\omega\tau}\exp[-Q(\tau)/\pi\hbar] \quad (19)$$

This Fourier transform appears in the transition probabilities given by eqs 13 and captures the effect of the bath in promoting

nonadiabatic transitions. As shown below, the bath favors transitions between vibronic or electronic states with energy differences corresponding to the region where the Fourier transform $I(\omega)$ is nonzero.

In this work, we choose the bath spectral density to have Ohmic form with an exponential cutoff[59]

$$J(\omega) = \eta\hbar\omega e^{-\omega/\omega_c} \tag{20}$$

This model is specified by the cutoff frequency ω_c and the unitless system−bath coupling strength η. In general, the solvent reorganization energy is defined as $\lambda_s = (1/\pi)\int_0^\infty d\omega J(\omega)/\omega$. For this particular bath spectral density, the solvent reorganization energy is $\lambda_s = \hbar\eta\omega_c/\pi$. Moreover, an exact analytical expression can be derived for $Q(\tau)$ for the Ohmic spectral density given in eq 20:

$$Q(\tau) = \eta\hbar \ln(1 + i\omega_c\tau) - \eta\hbar \ln\left[\Gamma\left(\Omega + \frac{i\tau}{\hbar\beta}\right)\Gamma\left(\Omega - \frac{i\tau}{\hbar\beta}\right)/\Gamma^2(\Omega)\right] \tag{21}$$

where $\Omega = 1 + 1/\hbar\beta\omega_c$ and $\Gamma(z)$ is the Euler gamma function[65] of a complex variable. The transition probability elements for the ultrafast interfacial ET and PCET models discussed below are computed using this exact expression.

In the calculations presented below, the conduction band states of the semiconductor are discretized. The density of states in the conduction band is given by

$$\bar{\mathcal{N}}(E) = \sum_k \delta(E - \epsilon_k) \tag{22}$$

The electronic coupling V_{rk} between the molecular electronic state $|r\rangle$ and the conduction band states $|k\rangle$ is specified by the resonance decay width

$$\Gamma(E) = 2\pi \sum_k |V_{rk}|^2 \delta(E - \epsilon_k) \tag{23}$$

We choose the density of states to be a constant that is independent of the energy[45,66]

$$\bar{\mathcal{N}}(E) = \bar{\mathcal{N}} = N/(E_{max} - E_{min}) \tag{24}$$

where N is the number of conduction band states and E_{min} and E_{max} are the minimum and maximum energies, respectively, of the conduction band. Similarly, the electronic coupling is chosen to be a constant $V_{rk} = \bar{V}_e$. As a result, the resonance decay width Γ is independent of energy and is related to the electronic coupling by

$$\Gamma = 2\pi\bar{\mathcal{N}}\,\bar{V}_e^{\,2} \tag{25}$$

As shown previously,[43] discretization of the conduction band introduces nonphysical recurrence effects in the population decay dynamics. The recurrence effects become apparent after a recurrence time that is inversely proportional to the chosen energy spacing in the conduction band. Thus, choosing a small enough energy spacing can ensure that the artificial recurrence effects do not occur during the time scale of the population decay. Within this chosen recurrence time domain, the discretized states have been found to behave as a continuum.[43]

III. Results and Discussion

IIIA. Ultrafast Interfacial PCET. In this subsection, we study the process of ultrafast interfacial PCET using the RDM formalism. For proton transfer reactions,[67−71] typically the donor U^{I} and acceptor U^{II} proton potentials are each described by an asymmetric double-well potential, as depicted in Figure 1. For the model system calculations, we assume that the asymmetry of both double-well potentials is large and that the solvent does not significantly impact the proton potentials. Based on these assumptions, we approximate the three proton potentials U^0, U^{I}, and U^{II} as harmonic potentials with identical frequencies of $\omega_H = 3000\ cm^{-1}$ for hydrogen and $\omega_D = \omega_H/\sqrt{2}$ for deuterium. Because the typical distance between the reactant and product minima for proton transfer reactions is ∼0.5 Å, the U^{I} and U^{II} minima are located at 0 and −0.5 Å, respectively.

We consider three different models characterized by the location of the minimum of U^0: in model A, the proton potential U^0 is the same as the acceptor state potential U^{II}; in model B, the proton potential U^0 is similar to the donor potential U^{I} and has a minimum at −0.15 Å; in model C, the proton potential U^0 is the same as the donor state potential U^{I}. In model A, the relatively large displacement between the proton potentials before and after photoexcitation results in an initial population concentrated among the higher vibronic states of the donor electronic state. In both models B and C, U^0 is close to U^{I}, leading to an initial population distribution among the lower vibronic states of the donor electronic state. All three models could correspond to the type of system in which the electron is photoexcited from the ground molecular electronic state to an excited molecular electronic state. In particular, models B and C correspond to the situation in which the ground and excited molecular electronic states are associated with very similar proton potentials, and model A corresponds to the situation in which these proton potentials are quite different. In addition, model A could represent the type of system in which the electron is photoexcited from the defect band in the semiconductor to a molecular adsorbate layer because the proton potentials associated with the transferring electron in the defect band and in the conduction band are expected to be the same, although this is not necessarily the case.

We choose system and bath parameters that are consistent with the underlying assumptions of the theoretical formalism. The solvated electron interacts strongly with the bath,[63] and we choose a large enough system−bath coupling to ensure efficient energy exchange between the bath and the system. The bath cutoff frequency is chosen to be larger than the electronic coupling (i.e., $\hbar\omega_c > \bar{V}_e$)[72,73] to ensure that the bath relaxes on a faster time scale than the electronic population decays. The parameters for the bath are $\omega_c = 600\ cm^{-1}$ and $\eta = 12\pi$, corresponding to a solvent reorganization energy of $\lambda_s = 0.892$ eV. The interaction between the molecular electronic state and the semiconductor electronic states is treated perturbatively, so the electronic coupling is chosen to be smaller than the energy spacing between the discretized conduction band states.[74] The width of the conduction band is chosen to be 2.7 eV, which approximately corresponds to the bandwidth of TiO_2.[75,76] The conduction band extends from 0 to 2.7 eV and consists of $N = 68$ equally spaced discretized states. The electronic coupling $\bar{V}_e$ is chosen to be 0.03 eV, which is smaller than the spacing 0.04 eV between the discretized conduction band states. We consider two different choices for the energy of the donor electronic state: $\epsilon_r = 1$ and 0.3 eV.

To propagate the RDM elements in time, the master equation given in eq 12 was cast in the form

$$\frac{\partial}{\partial t}\vec{P}(t) = \mathbf{L}\vec{P}(t) \tag{26}$$

where the relaxation matrix $\mathbf{L}$ is composed of the transition probabilities $W_{r\mu,k\nu}$ and $W_{k\nu,r\mu}$, and $\vec{P}(t)$ is the column vector

with elements $\sigma_{r\mu,r\mu}(t)$ and $\sigma_{kv,kv}(t)$. The solution to the above equation is[77]

$$\vec{P}(t) = e^{\mathbf{L}t}\vec{P}(0) = \mathbf{J}e^{\mathbf{D}t}\mathbf{J}^{-1}\vec{P}(0) \quad (27)$$

where **J** is the eigenvector matrix and **D** is the eigenvalue matrix of the diagonalizable matrix **L**. The population of each state obtained from this approach is a sum of exponential terms. The number of proton vibrational states required for convergence is determined by the temperature and the displacement between the donor and acceptor proton potentials. For each model, we included enough vibrational states to ensure that the donor state population is unity at zero time and that the trace of the RDM is conserved during the time propagation. We included 30 vibrational states for hydrogen and 35 vibrational states for deuterium for each electronic state at $T = 300$ K.

We also examined the relative time scales of the various processes occurring in the model systems to verify the validity of the underlying approximations in the theoretical formalism. We found that our choice of bath parameters ensures that the bath correlation function given by eq 17 decays to zero by 8 fs at $T = 300$ K and by 4 fs at $T = 2000$ K. Similarly, we found that all time-dependent transition probability elements $W_{r\mu,kv}$ and $W_{kv,r\mu}$ reach their stationary values by $t = 8$ fs. For all situations of interest in this work, the population decay time scales are longer than 8 fs, thereby validating our use of both the Markovian and stationary Redfield approximations.

1. H/D Isotope Effect on the Population Dynamics. We studied the population decay dynamics of the donor electronic state for the PCET process with both hydrogen and deuterium. Note that only the transferring nucleus is deuterated and the bath parameters are kept the same for both hydrogen and deuterium transfer. In this subsection, we analyze the results for all three models at $T = 300$ K and $\epsilon_r = 1$ eV.

As shown in Figure 3a, model A exhibits virtually no isotope effect for the entire duration of the population decay. This observation can be understood in terms of the relative time scales of the donor electronic state population decay and proton vibrational relaxation. Figure 4 depicts the populations of the hydrogen and deuterium vibrational states corresponding to the donor electronic state at times $t = 0$, 100, and 200 fs. Because of the large displacement between the ground and donor proton potentials in model A, the initial population is distributed over highly excited vibrational states in the U^{I} proton potential. The vibrational state with greatest population at zero time is $\mu = 11$ for hydrogen and $\mu = 15$ for deuterium. This difference between H and D is due to differing values of the Franck−Condon overlaps for the H and D vibrational wave functions. Figure 3a indicates that the population of the donor electronic state decays substantially by $t = 100$ fs. This fast decay time is due to the large number of acceptor electronic states in the semiconductor conduction band. As shown in Figure 4b, the population at this time is distributed mainly over higher vibrational states. The population is not concentrated in the lower vibrational states until $t \approx 200$ fs. Thus, the process of proton vibrational relaxation occurs on a time scale of ~200 fs, but by this time, the population of the donor electronic state is already nearly zero.

As discussed in ref 58 in the context of ultrafast homogeneous PCET, the population decay dynamics starts to exhibit an isotope effect only after proton vibrational relaxation has occurred, resulting in the localization of the proton wavepacket in the region of the U^{I} minimum. The models in the previous study of ultrafast homogeneous PCET included only a single acceptor electronic state, so the population decay occurred on the picosecond rather than the femtosecond time scale, but the underlying physical principles are similar. When the proton vibrational population in the donor state is distributed among higher vibrational states and the donor proton wavepacket is oscillating with large amplitude, the electronic state population dynamics exhibits virtually no hydrogen/deuterium isotope effect. After vibrational relaxation, the proton vibrational population in the donor state becomes concentrated in the lower vibrational states, the oscillations of the donor proton wavepacket are damped, and the donor proton wavepacket is localized near the minimum of the donor potential, so a significant hydrogen/deuterium isotope effect on the electronic state population dynamics is exhibited. Figures 3a and 4 indicate that proton vibrational relaxation within the donor electronic state is slow relative to the time scale of the donor electronic state population decay. By the time this proton vibrational relaxation occurs, the population of the donor electronic state is nearly zero, so no isotope effect is observed.

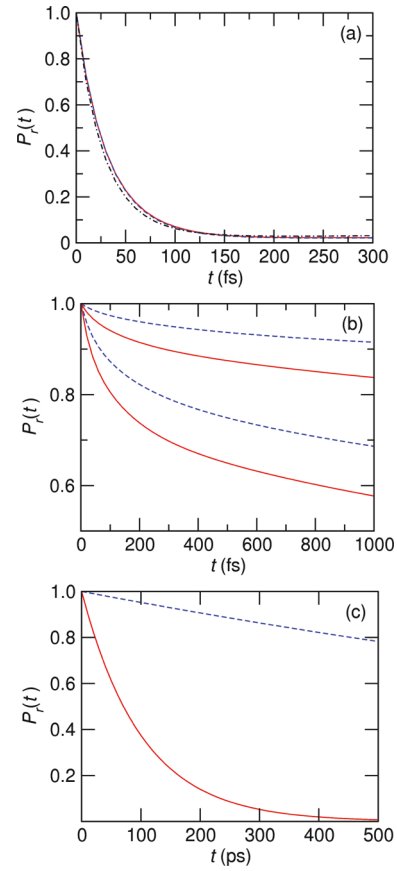

Figure 3. Population decay of the donor electronic state at $T = 300$ K for (a) model A, (b) model B, and (c) model C. For model A, the decay is depicted for H (red solid line) and D (blue dashed line) with $\epsilon_r = 1$ eV and for H (black dashed-dotted line) with $\epsilon_r = 0.3$ eV. For model B, the decay is depicted for H (red solid lines) and D (blue dashed lines) with $\epsilon_r = 1$ eV (lower curves) and $\epsilon_r = 0.3$ eV (upper curves). For model C, the decay is depicted for H (red solid line) and D (blue dashed line) with $\epsilon_r = 1$ eV.

In model B, the initial proton wavepacket is localized near the U^{I} minimum. Analysis of the vibrational states at zero time for hydrogen and deuterium indicates that the initial population is distributed among only the lowest six vibrational states with the maximum population in the first excited state (i.e., $\mu = 1$). In this case, the proton wavepacket is initially localized near the U^{I} minimum and becomes localized near the U^{II} minimum at long times. As shown in Figure 3b, model B exhibits a significant isotope effect on the population decay, where

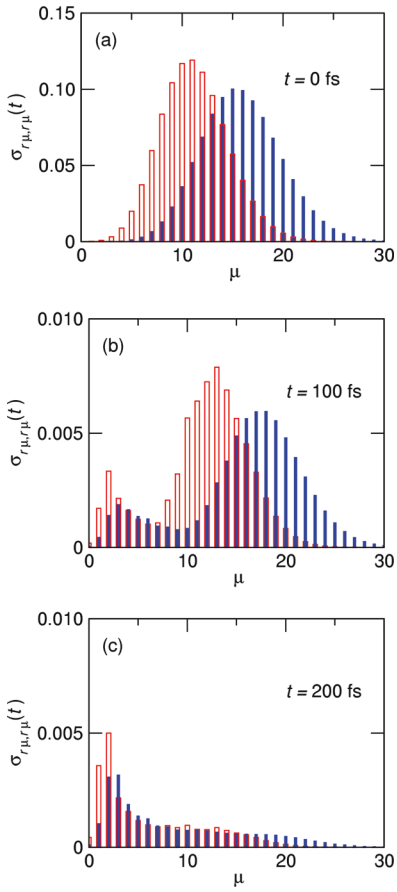

Figure 4. Population distribution among the H (red) and D (blue) vibrational states in the donor electronic state at t = (a) 0, (b) 100, and (c) 200 fs for model A at T = 300 K with ϵ_r = 1 eV.

hydrogen decays faster than deuterium. Moreover, the population decay time scale is notably slower for model B than for model A. This slower decay might be due to the smaller Franck−Condon overlaps associated with the lower vibrational states. These observations are consistent with previous studies of homogeneous PCET, where this type of model exhibited a pronounced isotope effect and a slower population decay.

As shown in Figure 3c, the population decay for model C also shows a significant isotope effect and occurs on an even slower time scale. For both hydrogen and deuterium, the initial population is almost entirely in the ground vibrational state at this temperature. The physical basis for the slow decay and the isotope effect is the same for model C as for model B.

2. Impact of the Donor Electronic state Energy on the Population Dynamics. The energy of the molecular electronic state with respect to the conduction band minimum varies for different dye molecules and molecular adsorbates. To study the impact of the donor electronic state energy ϵ_r on the population dynamics, we compared the results for models with ϵ_r = 0.3 eV, which is closer to the conduction band minimum, to the results with ϵ_r = 1.0 eV given in the previous subsection. For ϵ_r = 1.0 eV, ∼24 conduction band electronic states are below ϵ_r, and for ϵ_r = 0.3 eV, only ∼7 conduction band electronic states are below ϵ_r.

We found that ϵ_r does not significantly impact the qualitative isotope effect on the population decay dynamics. Specifically, we do not observe an isotope effect on the population decay for either value of ϵ_r for model A, and we do observe a distinct isotope effect for both values of ϵ_r for model B, as illustrated in Figure 3b. Because ϵ_r does not play a significant role in proton

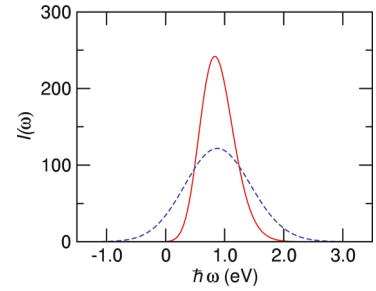

Figure 5. Fourier transform of the bath correlation function at T = 300 K (red solid line) and T = 2000 K (blue dashed line).

vibrational relaxation, it is not expected to impact the presence or absence of an isotope effect.

We also analyzed the impact of ϵ_r on the time scale of the population decay for hydrogen. Figure 3a illustrates that the H population decay time scales are approximately the same with ϵ_r = 1.0 eV and ϵ_r = 0.3 eV for model A. In contrast, Figure 3b illustrates that the H population decay is considerably faster with ϵ_r = 1.0 eV than with ϵ_r = 0.3 eV for model B. This behavior can be interpreted in terms of the dependence of the transition probabilities on the bath correlation function. Figure 5 depicts the functional form of $I(\omega)$, which is the Fourier transform of the bath correlation function. This quantity, which is defined in eq 19, impacts the transition probabilities given by eq 13. Figure 5 illustrates that the effect of the bath is to allow only transitions for which the difference between the energies of the initial and final states is between 0 and ∼2 eV for T = 300 K, where the most probable transitions occur for an energy difference of approximately λ_s = 0.892 eV. The time scale of the initial state population decay becomes faster as the number of acceptor vibronic states within this energy window increases. Note that a vibronic manifold for each acceptor electronic state in the conduction band is present, leading to many acceptor vibronic states of similar energies. The relative magnitudes of the transition probabilities are determined by the Franck−Condon overlaps, as well as the magnitude of $I(\omega)$.

The results of both models A and B can be understood in the context of these energetic restrictions. In model B, the initial population is distributed among vibronic states with energies smaller than the conduction band maximum for both ϵ_r = 1.0 eV and ϵ_r = 0.3 eV. The larger donor electronic state energy ϵ_r = 1.0 eV results in a larger number of accessible vibronic states within the energy window because more conduction band states can contribute. As a result, the population decay is faster for ϵ_r = 1.0 eV. In model A, however, the initial population distribution is concentrated well above the conduction band maximum for either value of ϵ_r. In this case, the number of energetically accessible vibronic states within the energy window is approximately the same for both values of ϵ_r because every conduction band state contributes approximately the same number of energetically accessible vibronic levels. As a result, the population decay time scales are similar for ϵ_r = 0.3 eV and ϵ_r = 1.0 eV for model A.

3. Effects of Electronic Coupling and Temperature on Population Dynamics. We also studied the impact of electronic coupling and temperature on the population decay of the donor electronic state for H and D. As is evident from eq 13, which shows that the transition probabilities are proportional to $\bar{V}_e^2$, reducing the electronic coupling leads to a slower population decay time scale. Changing the temperature from T = 300 K to T = 2000 K did not change the population decay time scale appreciably for model A. For models B and C, however,

increasing the temperature to $T = 2000$ K leads to a faster decay time scale for both H and D.

These results can be understood in the context of the impact of temperature on the Fourier transform of the bath correlation function, which, in turn, affects the transition probabilities. As shown in Figure 5, the energy window dictating the allowed transitions is wider for $T = 2000$ K than for $T = 300$ K, reflecting the more efficient energy exchange between the system and the bath at higher temperatures. In model B, the initial population is distributed among the lower proton vibrational states with energies smaller than the conduction band maximum. The wider range of energetically accessible vibronic states leads to a faster decay at $T = 2000$ K because more of the vibronic states with larger Franck−Condon overlaps can contribute to the overall decay process. In model A, the initial population is distributed in higher proton vibrational states concentrated above the conduction band maximum. In this case, the dominant Franck−Condon overlaps are relatively constant over the region of energetically accessible states, so the population decay is not significantly affected by the width of $I(\omega)$. As a result, the population decay rates are comparable at the two temperatures for model A.

IIIB. Ultrafast Interfacial ET. In this subsection, we examine the process of ultrafast interfacial ET and study the effects of temperature and donor state energy on the population decay. The parameters for the conduction band, the bath, and the electronic coupling are identical to those used for the PCET model. A fundamental difference between ultrafast interfacial PCET and ET is that the PCET system has a manifold of vibronic states associated with the donor electronic state and all acceptor electronic states. These manifolds of vibronic states extend far beyond the conduction band maximum. In the case of ET, however, all of the electronic states lie between the conduction band minimum and maximum. As a result, the dependence of the population decay on temperature and donor state energy is qualitatively different for interfacial PCET and ET.

The temperature effects are determined primarily by the bath contributions to the transition probabilities. The transition probability from the donor state to the kth acceptor state is proportional to the value of the Fourier transform $I(\omega)$ of the bath correlation function at the frequency corresponding to $\hbar\omega_{rk} = \epsilon_r - \epsilon_k$. As illustrated in Figure 5, $I(\omega)$ has a maximum at approximately $\lambda_s = 0.892$ eV for both $T = 300$ K and $T = 2000$ K, but the distribution is wider for the higher temperature. This behavior indicates that more acceptor states are energetically accessible (i.e., the transition probability is nonzero for more acceptor states) for the higher temperature. On the other hand, the maximum value of $I(\omega)$ is larger for the lower temperature, resulting in greater individual transition probabilities for the narrower band of energies. Furthermore, $I(\omega)$ extends to negative energies for the higher temperature, so acceptor states with higher energy than the donor state are accessible. This behavior is illustrated by Figure 6, which depicts the donor and acceptor electronic state populations at $t = 10$ and 50 fs for $\epsilon_r = 1$ eV. Whereas individual populations of some acceptor states are higher at $T = 300$ K, the population distribution is wider at $T = 2000$ K. This figure also illustrates that the acceptor state with the maximum population has an energy of approximately $\epsilon_r - \lambda_s$, corresponding to the location of the maximum of $I(\omega)$ (i.e., to the most probable transition).

The rate of population decay from the donor state is determined by a balance between the number of accessible states and the individual transition probabilities. Neglecting back

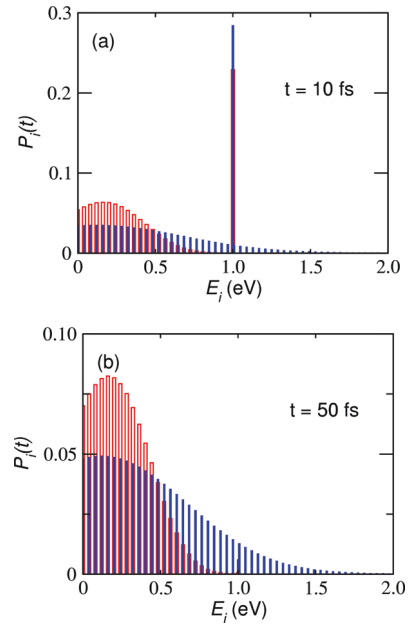

Figure 6. Population of the donor electronic state and conduction band acceptor electronic states at $t =$ (a) 10 and (b) 50 fs for electrochemical ET with $\epsilon_r = 1$ eV and $T = 300$ K (red) and $T = 2000$ K (blue). The donor electronic state population is depicted at $\epsilon_r = 1$ eV.

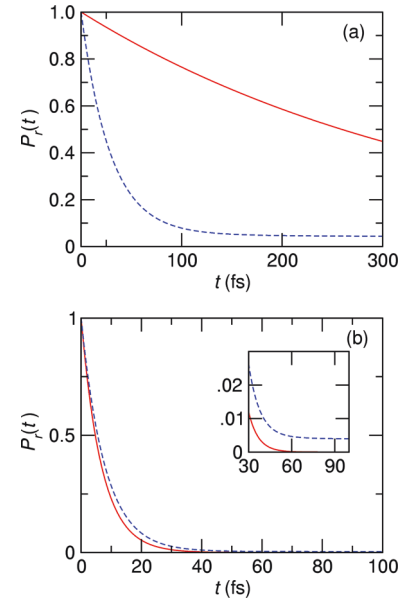

Figure 7. Population decay of the donor electronic state for electrochemical ET at $T = 300$ K (red solid line) and $T = 2000$ K (blue dashed line) for $\epsilon_r =$ (a) 0.3 and (b) 1 eV.

transfers for the purpose of analysis, the total transition probability from the donor electronic state is proportional to $\sum_k I(\omega_{rk})$ at short time. For small conduction band spacing, this probability is proportional to the integral of $I(\omega)$ between $\epsilon_r - E_{max}$ and ϵ_r. Thus, for a given value of ϵ_r, the area under the graph of $I(\omega)$ to the left of ϵ_r provides an estimate of the relative time scale of the donor state population decay. Figure 5 indicates that, for $\epsilon_r = 0.3$ eV, this area is larger for $T = 2000$ K than for $T = 300$ K. Thus, we expect a faster decay at the higher temperature for $\epsilon_r = 0.3$ eV. For $\epsilon_r = 1.0$ eV, however, the area is slightly larger for $T = 300$ K, so we expect a faster decay at the lower temperature. Figure 7 illustrates these trends in the population decay rates. Note that, for large values of ϵ_r that are near the conduction band maximum, the areas are

almost equal for the two temperatures and the donor state population decays are nearly identical for 300 and 2000 K. Figure 7 also indicates that, for fixed temperature, increasing the energy ϵ_r of the donor electronic state leads to a faster population decay because increasing ϵ_r leads to a larger number of accessible conduction band states.

At infinite time, the populations of the electronic states will reach the correct Boltzmann distribution, as ensured by the detailed balance condition. For fixed ϵ_r, the asymptotic limit of the donor state population depends on temperature. The inset in Figure 7b illustrates this deviation between the final populations at $T = 300$ and 2000 K for $\epsilon_r = 1$ eV.

IV. Conclusion

In this work, we studied the dynamics of photoinduced PCET at molecule−semiconductor interfaces. We described the PCET process with a model Hamiltonian in which the electronic states are coupled to a harmonic bath and the proton potentials associated with the donor and acceptor electronic states are represented by shifted harmonic potentials. A canonical transformation of the Hamiltonian allowed for the treatment of the strong coupling between the electronic states and the bath. We derived the equations of motion for the RDM elements in the basis of electron−proton vibronic states and used these equations to calculate the time-dependent electronic and vibronic state populations for a series of model systems. The theoretical formalism employed in this work is restricted to weak electronic coupling between the molecular electronic state and the semiconductor conduction band states, strong coupling between the electronic states and the bath, and fast bath relaxation relative to the population decay dynamics.

The model systems were designed to encompass situations in which the electron is photoexcited from the ground state to the excited electronic state within a dye molecule at the dye−semiconductor interface and situations in which the electron is photoexcited from the defect band in the semiconductor to a molecular adsorbate layer. In both cases, the initial nonequilibrium state is prepared by vertical photoexcitation from a lower-energy electronic state, leading to a coherent vibrational mixture in the donor electronic state. This nonstationary state relaxes to equilibrium through dynamical processes arising from nonadiabatic transitions between the donor and acceptor vibronic states concurrent with energy dissipation to the bath. When the proton potential associated with the electronic state prior to photoexcitation is shifted significantly with respect to the proton potential associated with the donor electronic state, the initial proton vibrational population in the donor state is distributed among higher vibrational states, and the proton wavepacket is oscillating with large amplitude. When these two proton potentials are similar, the initial proton vibrational population in the donor state is concentrated in the lower vibrational states, and the proton wavepacket is localized near the minimum of the donor proton potential.

Our model studies provide insight into the hydrogen/deuterium isotope effect on the dynamics of the donor state population decay for ultrafast interfacial PCET. As shown for photoexcited homogeneous PCET,[58] an isotope effect on the donor electronic state population decay is exhibited after the proton vibrational population has relaxed to the lower vibrational states and the proton wavepacket is localized near the minimum of the donor proton potential. For the photoinduced interfacial PCET models studied here, the electronic state population decay time scale is much faster than the proton vibrational relaxation time scale because of the large number of available conduction band acceptor states. As a result, an isotope effect on the donor electronic state population dynamics is not observed when the initial proton vibrational population is distributed among higher vibrational states but is observed when the initial proton vibrational population is concentrated in the lower vibrational states. In the case of photoinduced homogeneous PCET, where the electronic state population decay time scale is slower, we studied models in which the isotope effect is not evident at early times but appears at later times following proton vibrational relaxation. The models for interfacial PCET could be extended to describe this type of behavior by including a slow solvent coordinate or direct coupling between the proton and the bath so that proton vibrational relaxation occurs before the electronic state population dynamics is complete.

We also investigated the effects of the electronic coupling, temperature, and energy of the donor state on the population dynamics for photoinduced interfacial PCET. In general, the donor electronic state population decays faster as the electronic coupling increases. When the initial proton vibrational population is concentrated in the higher vibrational states for PCET, the donor electronic state population decay time scale is not significantly influenced by the temperature or the energy of the donor state. In contrast, when the initial proton vibrational population is concentrated in the lower vibrational states, the donor electronic state population decays faster as the temperature and the donor state energy are increased for these model systems.

For comparison, we also studied photoinduced interfacial ET using an analogous formalism. We found that increasing the energy of the donor electronic state relative to that of the conduction band minimum leads to faster decay of the donor state population because more acceptor states are energetically accessible. For fixed donor state energy, however, increasing the temperature could lead to either a faster or a slower decay of the donor state population, as determined by a balance between the number of accessible states and the individual transition probabilities.

The models studied in this work focus only on qualitative charge transfer dynamics and do not include the numerous complexities that are present in real molecule−semiconductor systems. The description of the semiconductor, including holes in the valence band and defects at the surface, is challenging. Moreover, the characterization of the solvated electron state in the molecular adsorbate layer and the nuclear rearrangements associated with the formation of this state is also challenging. These and other aspects of modeling the molecule−semiconductor interface require sophisticated computational methods that are beyond the scope of this work. On the other hand, even the simple models studied here can provide qualitative insights. For example, the present calculations provide a plausible explanation for the experimental observation of an isotope effect on the population dynamics for the slow component but not the fast component in the CH_3OH/TiO_2 system discussed in the Introduction.[16] Specifically, the present work indicates that the isotope effect is not observed for the fast component because the proton vibrational population is distributed among the higher proton vibrational states and the proton wavepacket is delocalized. The isotope effect is observed for the slow component because of proton vibrational relaxation, which leads to the concentration of the proton vibrational population in the lower proton vibrational states and localization of the proton wavepacket.

Theoretical predictions about the qualitative impact of altering system properties, such as the electronic coupling, donor state energy, and proton potentials, on the population decay time

scales could be useful for designing better catalysts. To broaden their applicability, these models could be extended to include a slow solvent coordinate and direct coupling between the proton and the bath. To avoid some of the approximations underlying the derivation of the equations of motion described above, these types of model systems could be studied with quantum dynamical methods, such as the multiconfigurational time-dependent Hartree method.[6] The combination of diverse theoretical approaches, in close connection with experimental studies, is important for the elucidation of the fundamental physical principles dictating the activation of bonds containing hydrogen atoms at surfaces.

Acknowledgment. We are grateful for support of this work by NSF Grant CHE-07-49646 and Grant CHE-08-02907 for POWERING THE PLANET: A Chemical Bonding Center in the Direct Conversion of Sunlight into Chemical Fuel.

References and Notes

(1) Hagfeldt, A.; Gratzel, M. *Acc. Chem. Res.* **2000**, *33*, 269.
(2) Gratzel, M. *Nature* **2001**, *414*, 338.
(3) Asbury, J. B.; Hao, E.; Wang, Y.; Ghosh, H. N.; Lian, T. *J. Phys. Chem. B* **2001**, *105*, 4545.
(4) Stier, W.; Prezhdo, O. V. *J. Phys. Chem. B* **2002**, *106*, 8047.
(5) Rego, L. G. C.; Batista, V. S. *J. Am. Chem. Soc.* **2003**, *125*, 7989.
(6) Thoss, M.; Kondov, I.; Wang, H. B. *Chem. Phys.* **2004**, *304*, 169.
(7) Kondov, I.; Thoss, M.; Wang, H. *J. Phys. Chem. A* **2006**, *110*, 1364.
(8) Kondov, I.; Cizek, M.; Benesch, C.; Wang, H.; Thoss, M. *J. Phys. Chem.* **2007**, *111*, 11970.
(9) Tsivlin, D. V.; Willig, F.; May, V. *Phys. Rev. B* **2008**, *77*, 035319.
(10) Duncan, W. R.; Prezhdo, O. V. *Annu. Rev. Phys. Chem.* **2007**, *58*, 143.
(11) Liu, S. H.; Miller, A. D.; Gaffney, K. J.; Szymanski, P.; Garrett-Roe, S.; Bezel, I.; Harris, C. B. *J. Phys. Chem. B* **2002**, *106*, 12908.
(12) Miller, A. D.; Bezel, I.; Gaffney, K. J.; Garrett-Roe, S.; Liu, S. H.; Szymanski, P.; Harris, C. B. *Science* **2002**, *297*, 1163.
(13) Onda, K.; Li, B.; Petek, H. *Phys. Rev. B* **2004**, *70*, 045415.
(14) Onda, K.; Li, B.; Zhao, J.; Jordan, K. D.; Yang, J. L.; Petek, H. *Science* **2005**, *308*, 1154.
(15) Onda, K.; Li, B.; Zhao, J.; Petek, H. *Surf. Sci.* **2005**, *593*, 32.
(16) Li, B.; Zhao, J.; Onda, K.; Jordan, K. D.; Yang, J. L.; Petek, H. *Science* **2006**, *311*, 1436.
(17) Zhao, J.; Li, B.; Jordan, K. D.; Yang, J. L.; Petek, H. *Phys. Rev. B* **2006**, *73*, 195309.
(18) Zhao, J.; Li, B.; Onda, K.; Feng, M.; Petek, H. *Chem. Rev.* **2006**, *106*, 4402.
(19) Tang, J.; Durrant, J. R.; Klug, D. R. *J. Am. Chem. Soc.* **2008**, *130*, 13885.
(20) Sebastian, K. L.; Chakraborty, A.; Tachiya, M. *J. Chem. Phys.* **2003**, *119*, 10350.
(21) Sebastian, K. L.; Chakraborty, A.; Tachiya, M. *J. Chem. Phys.* **2005**, *123*, 214704.
(22) Li, X.; Tully, J. C. *Chem. Phys. Lett.* **2007**, *439*, 199.
(23) Cheng, H. Z.; Shenvi, N.; Tully, J. C. *Phys. Rev. Lett.* **2007**, *99*, 053201.
(24) Cukier, R. I. *J. Phys. Chem.* **1996**, *100*, 15428.
(25) Cukier, R. I.; Nocera, D. G. *Annu. Rev. Phys. Chem.* **1998**, *49*, 337.
(26) Soudackov, A.; Hammes-Schiffer, S. *J. Chem. Phys.* **2000**, *113*, 2385.
(27) Hammes-Schiffer, S. *Acc. Chem. Res.* **2001**, *34*, 273.
(28) Soudackov, A.; Hatcher, E.; Hammes-Schiffer, S. *J. Chem. Phys.* **2005**, *122*, 014505.
(29) Hammes-Schiffer, S.; Soudackov, A. V. *J. Phys. Chem. B* **2008**, *112*, 14108.
(30) Venkataraman, C.; Soudackov, A. V.; Hammes-Schiffer, S. *J. Phys. Chem. C* **2008**, *112*, 12386.
(31) Navrotskaya, I.; Soudackov, A. V.; Hammes-Schiffer, S. *J. Chem. Phys.* **2008**, *128*, 244712.
(32) Navrotskaya, I.; Hammes-Schiffer, S. *J. Chem. Phys.* **2009**, *131*, 024112.
(33) Schmickler, W. *J. Electroanal. Chem.* **1986**, *204*, 31.
(34) Mohr, J.-H.; Schmickler, W. *Phys. Rev. Lett.* **2000**, *84*, 1051.
(35) Mohr, J.; Schmickler, W.; Badiali, J. P. *Chem. Phys.* **2006**, *324*, 140.
(36) Grimminger, J.; Schmickler, W. *J. Appl. Electrochem.* **2006**, *36*, 1231.
(37) Santos, E.; Koper, M. T. M.; Schmickler, W. *Chem. Phys. Lett.* **2006**, *419*, 421.
(38) Santos, E.; Koper, M. T. M.; Schmickler, W. *Chem. Phys.* **2008**, *344*, 195.
(39) Grimminger, J.; Schmickler, W. *Chem. Phys.* **2007**, *334*, 8.
(40) Sebastian, K. L. *J. Chem. Phys.* **1998**, *109*, 1111.
(41) Ramakrishna, S.; Willig, F. *J. Phys. Chem. B* **2000**, *104*, 68.
(42) Ramakrishna, S.; Willig, F.; May, V. *Phys. Rev. B* **2000**, *62*, R16330.
(43) Ramakrishna, S.; Willig, F.; May, V. *J. Chem. Phys.* **2001**, *115*, 2743.
(44) Wang, L. X.; Ernstorfer, R.; Willig, F.; May, V. *J. Phys. Chem. B* **2005**, *109*, 9589.
(45) Wang, L. X.; Willig, F.; May, V. *J. Chem. Phys.* **2007**, *126*, 134110.
(46) Sebastian, K. L.; Tachiya, M. *J. Chem. Phys.* **2006**, *124*, 064713.
(47) Anderson, P. W. *Phys. Rev.* **1961**, *124*, 41.
(48) Newns, D. M. *Phys. Rev.* **1969**, *178*, 1123.
(49) Schreiber, M.; Kondov, I.; Kleinekathofer, U. *J. Lumin.* **2001**, *94*, 471.
(50) May, V.; Kuhn, O.; Schreiber, M. *J. Phys. Chem.* **1993**, *97*, 12591.
(51) Wolfseder, B.; Domcke, W. *Chem. Phys. Lett.* **1995**, *235*, 370.
(52) Wolfseder, B.; Domcke, W. *Chem. Phys. Lett.* **1996**, *259*, 113.
(53) Egorova, D.; Kuhl, A.; Domcke, W. *Chem. Phys.* **2001**, *268*, 105.
(54) Egorova, D.; Domcke, W. *Chem. Phys. Lett.* **2004**, *384*, 157.
(55) Redfield, A. G. The theory of relaxation processes. In *Advances in Magnetic Resonance*; Waugh, J. S., Ed.; Academic Press: New York, 1965; Vol. 1; pp 1−32.
(56) Blum, K. *Density Matrix Theory and Applications*; Plenum Press: New York, 1996.
(57) Pollard, W. T.; Felts, A. K.; Friesner, R. A. The Redfield equation in condensed-phase quantum dynamics. In *New Methods in Computational Quantum Mechanics*; Prigogine, I., Rice, S. A., Eds.; Advances in Chemical Physics Series; Wiley Interscience: New York, 1996; Vol. 93; pp 77−134.
(58) Venkataraman, C.; Soudackov, A. V.; Hammes-Schiffer, S. *J. Chem. Phys.* **2009**, *131*, 154502.
(59) Weiss, U. *Quantum Dissipative Systems*; World Scientific: Singapore, 2008.
(60) Mahan, G. D. *Many Particle Physics*; Kluwer Academic/Plenum Publishers: New York, 2000.
(61) Leggett, A. J.; Chakravarty, S.; Dorsey, A. T.; Fisher, M. P. A.; Garg, A.; Zwerger, W. *Rev. Mod. Phys.* **1987**, *59*, 1.
(62) Egorova, D.; Thoss, M.; Domcke, W.; Wang, H. B. *J. Chem. Phys.* **2003**, *119*, 2761.
(63) Mosyak, A. A.; Prezhdo, O. V.; Rossky, P. J. *J. Chem. Phys.* **1998**, *109*, 6390.
(64) Schwartz, B. J.; Rossky, P. J. *J. Chem. Phys.* **1996**, *105*, 6997.
(65) Abramowitz, M.; Stegun, I. A. *Handbook of Mathematical Functions*; Dover Publications: New York, 1975.
(66) Shenvi, N.; Roy, S.; Parandekar, P.; Tully, J. C. *J. Chem. Phys.* **2006**, *125*, 154703.
(67) Borgis, D.; Hynes, J. T. *J. Chem. Phys.* **1991**, *94*, 3619.
(68) Hammes-Schiffer, S.; Tully, J. C. *J. Chem. Phys.* **1994**, *101*, 4657.
(69) Kim, S. Y.; Hammes-Schiffer, S. *J. Chem. Phys.* **2003**, *119*, 4389.
(70) Makri, N.; Miller, W. H. *J. Chem. Phys.* **1989**, *91*, 4026.
(71) Timoneda, J. J. I.; Hynes, J. T. *J. Phys. Chem.* **1991**, *95*, 10431.
(72) Egger, R.; Mak, C. H. *Phys. Rev. B* **1994**, *50*, 15210.
(73) Thoss, M.; Wang, H. B.; Miller, W. H. *J. Chem. Phys.* **2001**, *115*, 2991.
(74) Sakurai, J. J. *Modern Quantum Mechanics*; Addison-Wesley: New York, 1999.
(75) Kasowski, R. V.; Tait, R. H. *Phys. Rev. B* **1979**, *20*, 5168.
(76) Poumellec, B.; Durham, P. J.; Guo, G. Y. *J. Phys.: Condens. Matter* **1991**, *3*, 8195.
(77) Pollard, W. T.; Friesner, R. A. *J. Chem. Phys.* **1994**, *100*, 5054.

JP908798N